Repeatability of the Seasonal Variations of Ozone near the Mesopause from Observations of the 11.072-GHz Line

A. E. E. ROGERS,* P. ERICKSON,* V. L. FISH,* J. KITTREDGE,[+] S. DANFORD,[#] J. M. MARR,[@]
M. B. ARNDT,[&] J. SARABIA,** D. COSTA,** AND S. K. MAY[++]

* MIT Haystack Observatory, Westford, Massachusetts
[+] Chelmsford High School, Chelmsford, Massachusetts
[#] University of North Carolina at Greensboro, Greensboro, North Carolina
[@] Union College, Schenectady, New York
[&] Bridgewater State University, Bridgewater, Massachusetts
** Lynnfield High School, Lynnfield, Massachusetts
[++] Middlesex School, Concord, Massachusetts

ABSTRACT

Ground-based observations of the 11.072-GHz line of ozone were made from January 2008 through the middle of September 2011 to estimate the maximum in the nighttime ozone in the upper mesosphere at an altitude of about 95 km for a region centered at 38°N, 290°E. The measurements show seasonal variation with a high degree of repeatability with peaks in ozone concentration about a month following each equinox. A significant increase in ozone concentration above the yearly trend occurred in 2010 from mid-November until the end of December, which the authors attribute to delay in the start of the meridional circulation for the austral summer of 2010.

1. Introduction

Ground-based observations of the relatively weak microwave line of ozone at 11.072 454 5 GHz (Pickett et al. 1998) in the upper mesosphere using low-cost satellite TV electronics have been made by the education project known as "The Mesospheric Ozone System for Atmospheric Investigations in the Classroom" (MOSAIC). Along with the primary goal of providing locally acquired data to aid in the teaching of data analysis methods and statistics to high school students, MOSAIC provides an ongoing source of data on mesospheric ozone, which is publicly available online (at www.haystack.mit.edu/ozone). The ozone in the upper mesosphere is measured by MOSAIC using a satellite TV low-noise block downconverter followed by an intermediate frequency downconverter and analog-to-digital converter. The antenna, at each participating site, is directed at an elevation of 8° toward a region at 38°N, 290°E where the beam intersects the upper mesosphere.

The ozone at this altitude is observed as a relatively narrow line where the width is dominated by the thermal Doppler broadening, thereby allowing separation from the ozone at lower altitudes, which is predominantly pressure broadened. The ozone concentration in the upper mesosphere is estimated from the amplitude of a model spectrum, derived from radiative transfer of the thermal emission due to the line optical depth, which fits the observed spectra best in a least squares sense. The spectrum is derived by a fast Fourier transform of the digitized data and returned via the Internet. A simplified block diagram of the ozone spectrometer is shown in Fig. 1a.

A complete description of the instrument along with measurements of the seasonal and diurnal variations of ozone near the mesopause for data of 2008 was reported by Rogers et al. (2009) and the details of the model spectra fit to the data are described in the next section. In this paper we extend the results of Rogers et al. (2009) to cover more than 3 years of data during which additional sites were added.

A strong motivation for the study of mesospheric ozone is the potential for the study of the interhemispheric circulation (Houghton 2007) in the mesosphere. In this
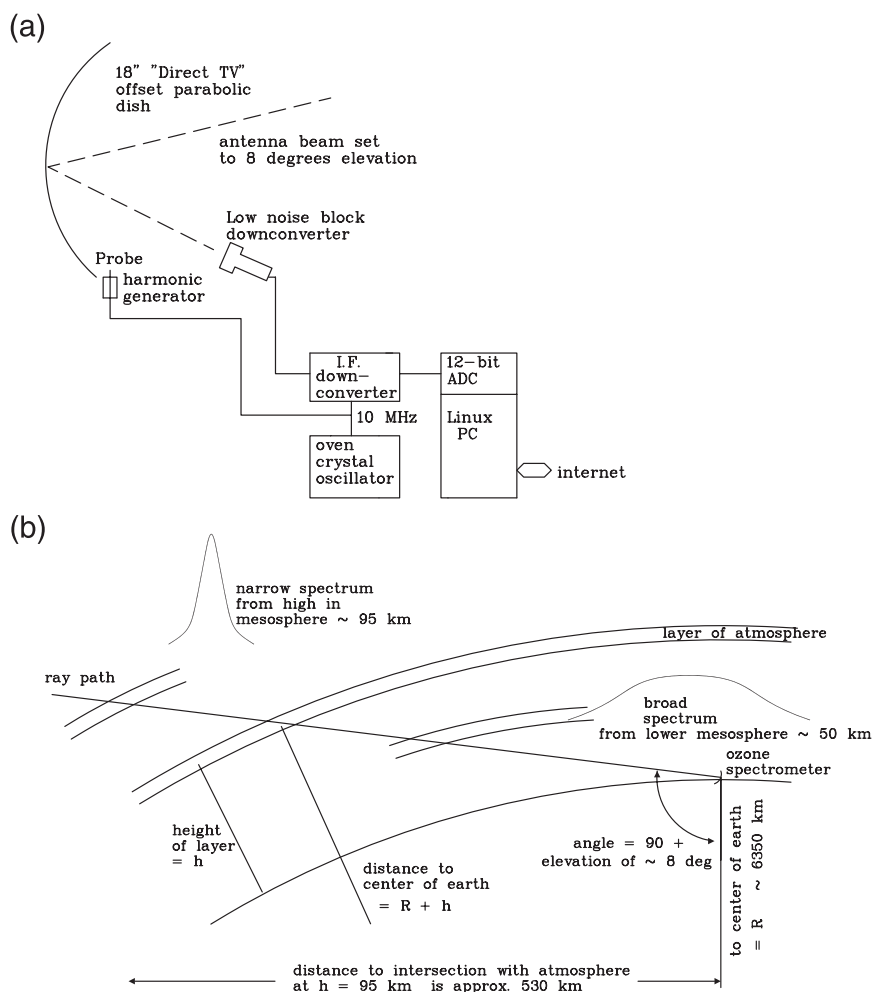
(a)

(b)

FIG. 1. (a) Simplified block diagram of the ozone spectrometer. The oven crystal oscillator provides an accurate frequency reference for the downconverter and sampler as well as injecting harmonics of 10 MHz in the spectrum to correct the frequency of the local oscillator in the low-noise block downconverter. (b) Geometry of the ray path though the earth's atmosphere that results in the spectrum seen by the MOSAIC spectrometer.

circulation of the upper atmosphere there is meridional flow from the summer to the winter pole via the mesosphere with reversal at the equinoxes. The simple chemistry of the ozone in the mesosphere makes its concentration largely dependent on the atomic hydrogen from the photodissociation of water vapor (Smith and Marsh 2005).

2. 11-GHz ozone spectrometers

The data reported here were obtained from six spectrometers located at the sites given in Table 1. The data for five of the six sites were obtained for a period of almost 3 years with less than 1 week of data at each site

TABLE 1. Locations of 11-GHz spectrometers. The last day included was 12 Sep 2011.

Spectrometer location	Town	State	Lat (°N)	Lon (°E)	Start date	Site
Chelmsford High School	Chelmsford	MA	42.62	288.63	26 Jan 2008	1
Haystack Observatory	Westford	MA	42.60	288.53	4 Jul 2008	2
Bridgewater State University	Bridgewater	MA	41.99	288.99	27 Jan 2009	3
Union College	Schenectady	NY	42.80	286.07	14 Apr 2009	4
Univ. of North Carolina	Greensboro	NC	36.07	280.17	20 Jun 2009	5
Lynnfield High School	Lynnfield	MA	42.54	288.97	6 Aug 2010	6

TABLE 2. Observing parameters.

Observing parameter		Comments
Spectrometer resolution	9.8 kHz	Smoothed from 4.9 kHz
No. of spectral points	64	
System noise temp	100 K	
1-sigma rms noise	5 mK	For 24 observing hours with a single spectrometer
1-sigma rms noise	3.5 mK	For 8 h using six spectrometers

lost because of power failures or heavy rain. The data reported here starts 26 January 2008 with the first site and ends 12 September 2011 with all six sites operating. All spectrometers are pointed at an elevation of 8° ± 1° and with an azimuth that intersects the atmosphere at 100-km altitude about 400 km off the coast of Maryland at approximately 38°N, 290°E. The low elevation as illustrated in Fig. 1b is employed to increase the pathlength and hence the optical depth of the ozone in order to enhance the signal-to-noise ratio (SNR) of the weak 11-GHz line.

3. Observing and data analysis technique

The observing technique described by Rogers et al. (2009) was used with key parameters as summarized in Table 2.

Figure 2a shows a sample ozone spectrum for 10 days of nighttime data taken from all six sites, while Fig. 2b shows a sample ozone spectrum for a single night's data from the Haystack spectrometer. Despite the limited nightly sensitivity of a single spectrometer, the sensitivity of six spectrometers is 0.9 mK over 10 nights corresponding to an approximate error of 0.5 ppm by volume (ppmv) in the nighttime ozone near 95 km.

The ozone concentration expressed as a mixing ratio in units of ppmv for ozone above and below 80 km is derived by fitting a two-parameter model to the data as described in Rogers et al. (2009). The two-component approach consists of one model spectrum for a constant volume mixing ratio of ozone from 50 to 80 km and another model spectrum for a Gaussian distribution of mixing ratio full width at half maximum of 10 km centered at 95 km. This two-parameter model fits the spectral data within the noise as illustrated in Figs. 2a and 2b and provides the best height resolution achievable with the available SNR. This two-component modeling results in the retrieval of the average mixing ratio above 80 km weighted by the assumed Gaussian. For example, the model spectrum that fits the sample spectrum in Fig. 2a is that of a Gaussian with peak mixing ratio of 14 ppmv seen as the difference between the solid and the dashed curves.

(a)

(b)

2010_300 to 2010_310 Integ. 640.7 hrs 1_sigma 0.9 mK sun_elev. -68 to -10 deg
CHS Bridge Union UNCG LHS Haystack

2010_305 to 2010_305 Integ. 10.0 hrs 1_sigma 7.5 mK sun_elev. -66 to -10 deg
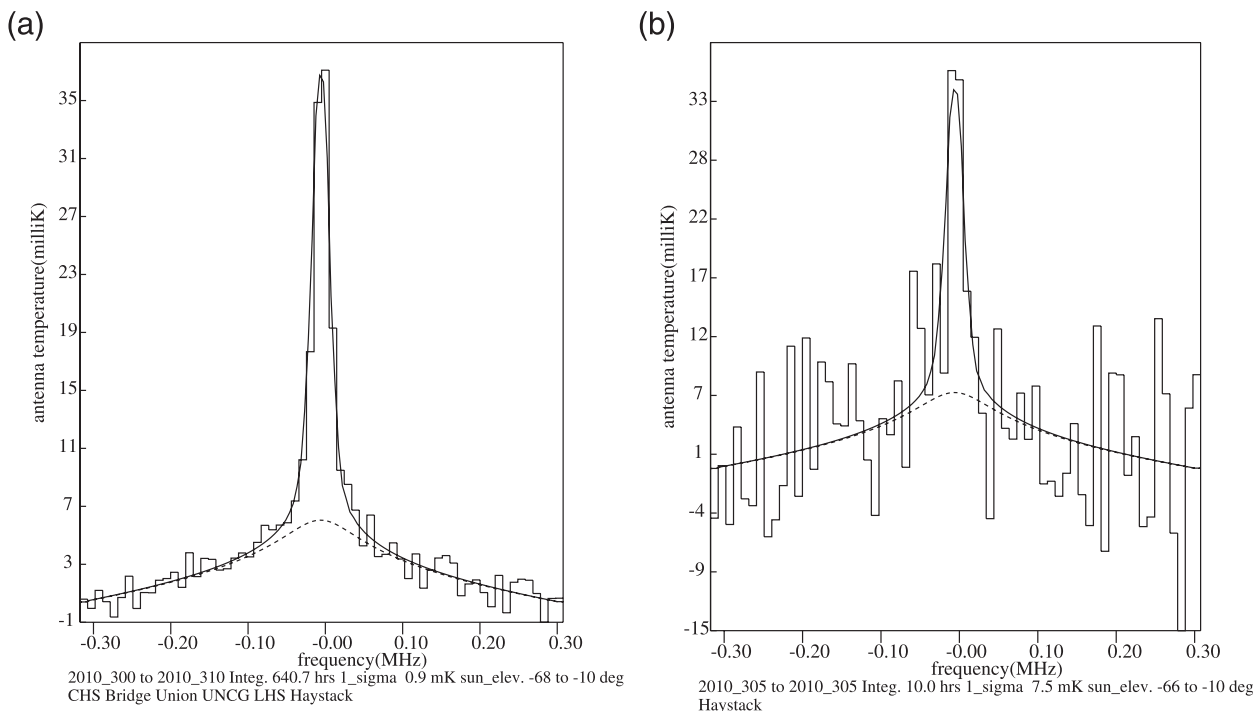Haystack

FIG. 2. (a) Spectrum of nighttime observations from all six sites from 27 Oct to 6 Nov 2010. The solid curve is the model fit to the data. The dashed curve and the difference between the solid and the dashed curves are the portions of the model for the ozone below and above 80 km, respectively. The two-component model fit to this data results in a peak volume mixing ratio of 14 ppmv of the assumed Gaussian profile for the ozone above 80 km. (b) Spectrum from a single night, 1 Nov 2010, at the Haystack site.
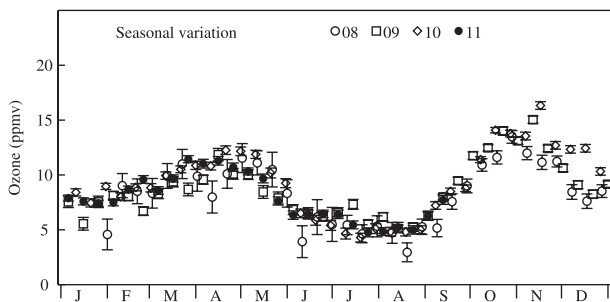
FIG. 3. Seasonal variation of mesospheric ozone concentration above 80 km for a region centered at 38°N. The error bars represent ±1 sigma. Data points are 10-day averages of all available sites.

The ozone concentration below 80 km is not well determined by the 11-GHz spectrometers, and so we limit the results in this paper to the ozone above 80 km. The model spectra are computed for the 11-GHz line using the spectroscopic data from the Jet Propulsion Laboratory (JPL) tables (Pickett et al. 1998). The line strength value of $10^{-6.9997}$ nm^2 MHz at 300 K, lower state energy of 8.0217 cm^{-1}, and the ratios of the total internal partition sums were used to obtain the line intensity corrected to 190 K using Eq. (A11) from Rothman et al. (1998). The instrumental spectral response width of 9.8 kHz was convolved with the line profile based on a collision line width of 2.6 MHz hPa^{-1} at 296 K, with a 0.71 temperature coefficient taken from the 2004 High-Resolution Transmission Molecular Database (HITRAN04: Rothman et al. 2005), and a Doppler line width and thermal emission assuming temperatures of 190 and 210 K above and below 80 km, respectively. A fixed relation between pressure and altitude with 0.001 hPa at 92 km was assumed for the conversion from volume mixing ratio to the concentration in number density.

Finally, the model spectra are derived by adding up the contributions of all the layers at different heights taking into account the geometry of the curved surface
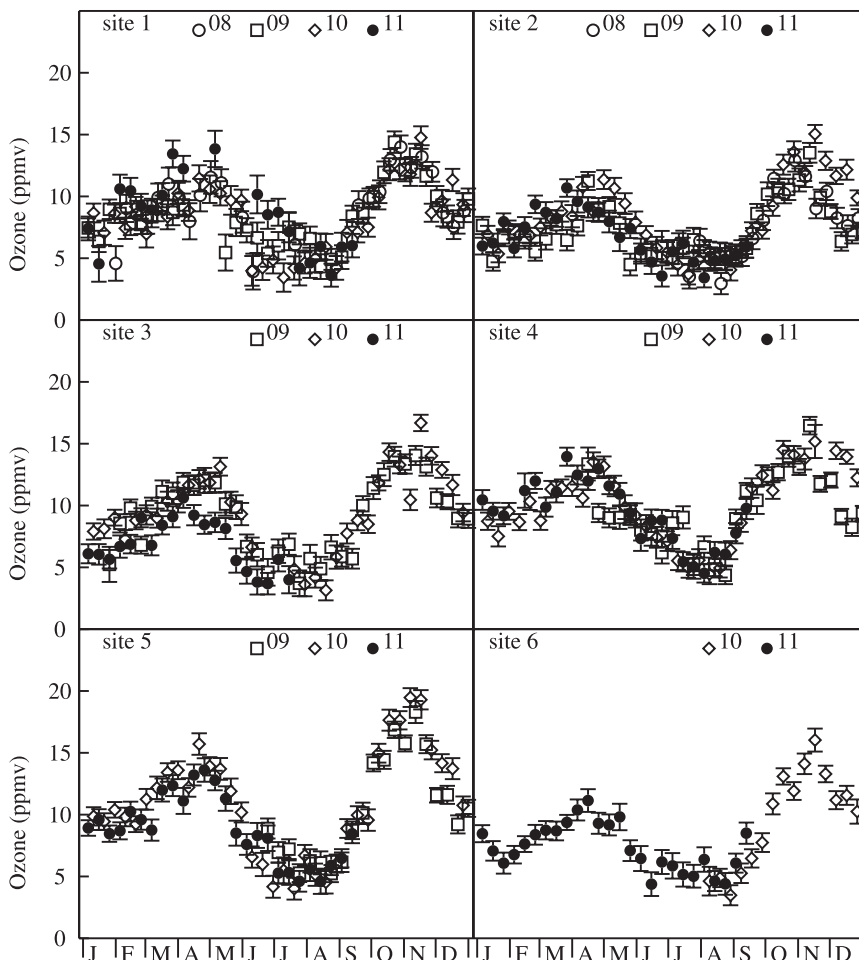

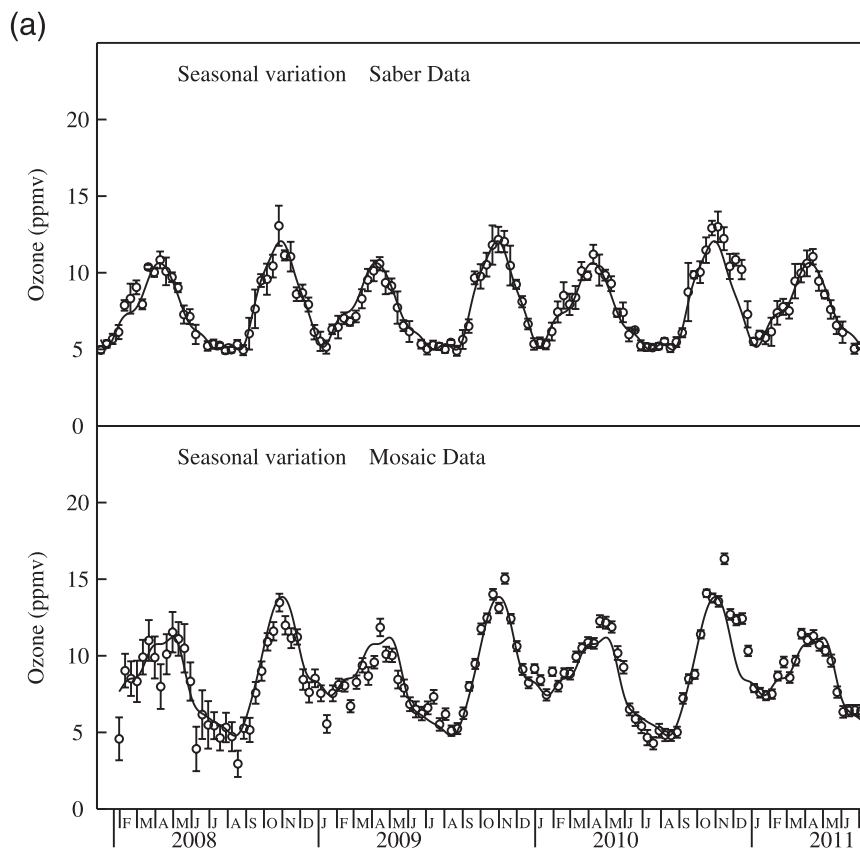FIG. 4. Seasonal variation shown for each site separately.

(a)

FIG. 5. a. Seasonal variation from all the available sites, as in Fig. 2. The solid curve is a 19-term Fourier series with a 1-yr period that was the best fit to all data excluding that from November and December 2010. For comparison we also show SABER data for a similar time period (see text for details). (b) Residual seasonal variation from all the available sites, after the removal of the best-fit 19-term Fourier series with a 1-yr period.

of the earth. We note that, in the calculations by Rogers et al. (2009), there was an arithmetic error in the conversion from number density to volume mixing ratio and an error in the temperature correction of the line intensity. These errors, which made the values of mixing ratio higher than they should have been by a factor of 2, have been corrected in the results reported in this paper. In addition we centered the Gaussian at 95 km rather than 92 km and changed the assumed temperature to 190 from 175 K. Both of these changes were made to make the Gaussian weighting and the temperature of the peak of the mixing ratio more consistent with the ozone data from the Sounding of the Atmosphere using Broadband Emission Radiometry (SABER) instrument aboard the *Thermosphere, Ionosphere, and Mesosphere Energetic and Dynamics (TIMED)* satellite. We assumed zero Doppler shift from winds in the mesosphere since the estimated frequency shifts are much smaller than the resolution. Details of the calculation of the model spectra from the

spectroscopic parameters of the 11 GHz line are given in the appendix.

4. Seasonal changes in ozone above 80 km

Figure 3 shows the seasonal variation of the mesospheric ozone concentrated above 80 km from 26 January 2008 through the middle of September 2011. The uncertainties are reduced results as the data from additional spectrometers are averaged, as indicated by the errors bars, which are based on the thermal noise. The data points are 10-day averages of all the available spectrometers plotted every 10 days for nighttime data, defined as when the sun was below $-10°$ elevation to ensure nighttime conditions at 100 km.

Figure 3 shows that the general seasonal variation repeats quite well from year to year, but some points in December 2010 are significantly higher than the usual seasonal variations. Figure 4 shows the averaged seasonal variation for each site separately, from which it is
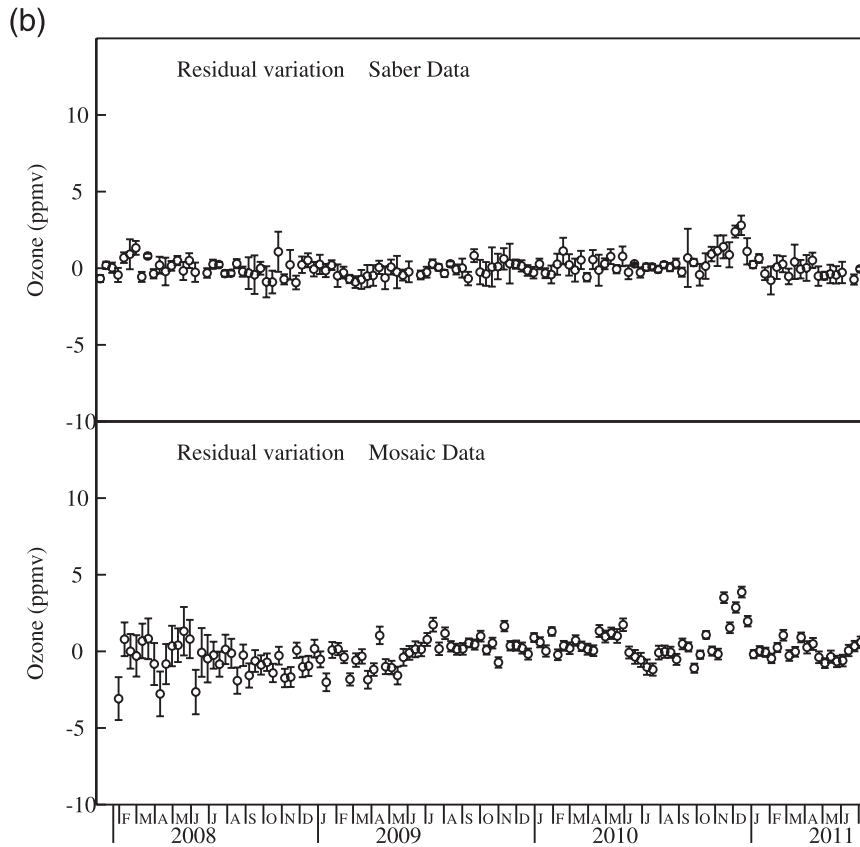
(b)

FIG. 5. (*Continued*)

apparent that the general seasonal trend is present in the data from each site and the data from December 2010 for sites 1 through 5 (site 6 was not in operation before 2010) are generally higher than other years (although only marginally so at sites 1 and 5).

In Fig. 5a the seasonal variation from all sites (as in Fig. 2) is plotted against time along with the best-fit Fourier series of a constant plus sine and cosine terms up to the ninth harmonic of a 1-yr period, and in Fig. 5b the residual seasonal variation is plotted after subtraction of the best-fit Fourier series. This series representation was needed to remove the long- and medium-term variations that are not well fit with only annual and semiannual terms.

For comparison we also plot in Fig. 5 the seasonal variation of ozone from SABER. The SABER data were obtained for a period from January 2008 through May 2011 for a latitude range of 37°–39°N. The results plotted are a weighted average for nighttime data (sun's elevation below −10°) for all longitudes. The altitude weighting function used was the same Gaussian (full width half maximum of 10 km centered at 95 km) as used for the model spectrum in the MOSAIC data. The points plotted are 10-day averages with errors taken from the standard deviation of the data from each day. A

few hundred out of the millions of data points in the SABER 1.07 data archive used for the plot in Fig. 5 had a mixing ratio over 100 ppmv. These data, most of which came from 3 January 2009, were assumed to be bad and were excluded from the average. The comparison of SABER and MOSAIC data is discussed further in the next section.

5. Sources of systematic error

There are a number of systematic errors associated with the MOSAIC data as follows in approximate order of increasing significance.

1) MOSAIC sites sample only approximately the same region of the mesosphere. However, all sites sample a region within 1° in latitude and longitude so the differences should be small. Furthermore, averages of the SABER data over longitude showed little change with a 1° change in latitude and no discernible change when averaging over different quadrants of longitude.

2) The conversion from the observed MOSAIC spectrum to the ozone concentration assumes the specific model described in section 3. While it is hard to
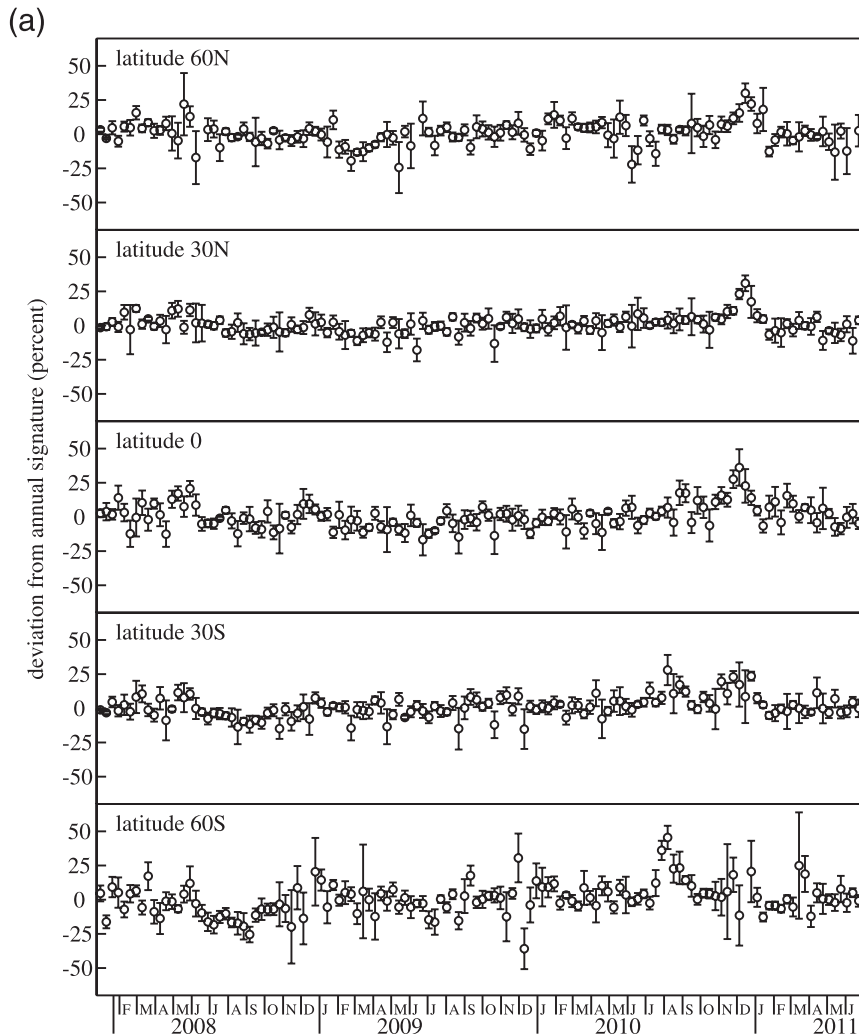
(a)

FIG. 6. (a) Fractional deviation of the mesospheric ozone from the annual signature obtained from SABER for 30° wide bands of latitude centered at 60°S, 30°S, 0°, 30°, and 60°N for an altitude of 95 km. The errors are from the standard deviation from the mean in each day of the 10 day average. (b) Deviation of ozone from the annual signature for each quadrant of longitude for a band of latitude from 30°S to 60°N at an altitude of 95 km. (c) Deviation of ozone from the annual signature for the global average at altitudes of 70, 80, and 90 km.

estimate the error introduced by the model, we note that a typical profile of ozone observed by SABER follows a mixing ratio with approximately Gaussian shape centered around 95 km with about 10 km full width at half maximum (Smith et al. 2008). The retrieval of the mixing ratio from MOSAIC measurements is also sensitive to the assumed temperature owing to the substantial change of line intensity with temperature. A decrease of 10 K in the assumed temperature from 190 to 180 K drops retrieved mixing ratio by about 10%. However, the temperature from the SABER data at 95 km at 38°N averaged over longitude is close to 190 K and shows no discernible seasonal variation at the level of 2 K.

3) MOSAIC spectrometers are not automatically calibrated and rely on a constant noise temperature of the low noise amplifier between infrequent manual calibrations using an absorber as a "hot load" and the sky as a "cold load" with an assumed temperature that is weather dependent. The absorber calibrations result in system noise temperatures close to 100 K for each spectrometer. A signal loss of 25% due to the "spillover" of the feed illumination of the dish results in an antenna beam efficiency of 75%, which is incorporated into the ozone mixing ratio estimates. The main effect of variations in spectrometer calibration is differences in scale between spectrometers, which remain constant with time.
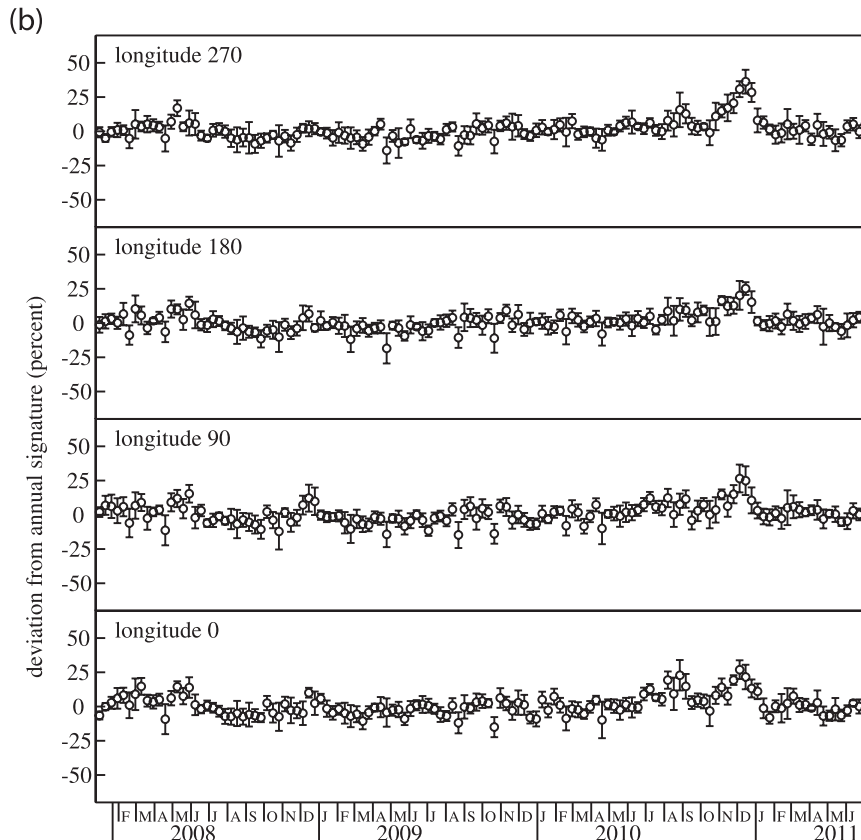
(b)

FIG. 6. (*Continued*)

4) Weather conditions affect the attenuation in the atmosphere of received signals measured by MOSAIC, and in the case of light rain there is added attenuation for which there is no correction. We have minimized these problems, though, since during heavy rain the noise temperature is raised by a large enough amount to be detected in the software, and which then excludes these data from the spectral averaging. A 1-dB increase was chosen as the criteria for the rejection of data due to rain.

The weather dependence is the largest source of MOSAIC systematic error especially on the short time scales associated with the tropospheric weather. The attenuation change at 11 GHz due to water vapor for a path through the troposphere at 8° elevation is estimated from Shambayati (2008) to go from 0.01 dB for extremely dry conditions to about 0.1 dB for 20 g m^{-3} surface water vapor density or 70% relative humidity at 30°C. A 0.1-dB increase in atmospheric attenuation raises the 100-K system noise by 7 K (7%) and reduces the signal by 2%, which results in a net decrease in the measured concentration by 9%. One advantage of distributed sites is that poor conditions are seldom present at all sites so that the average from all sites is less affected by the weather.

Considering these factors, we estimate that the sources of systematic error due to possible sampling of different regions, conversion of the spectra to concentration and uncertainty in calibration amount to ~10%. Adding this in quadrature to the typical noise brings the total estimate to ~15%, which is close to the level of the differences between the curves in Fig. 4. The actual error bars plotted in the figures are estimated from the noise alone. Some of the very low points for site 1 are the result of a combination of poor weather not excluded from the data and noise. Additionally, there are some variations in the ozone concentration derived from the data on time scales shorter than the plotted 10-day average. These variations may be significant but are not discussed in this paper.

6. Comparison with other data

Seasonal variation of mesospheric ozone showing maxima at the equinoxes was first reported from ground-based observations at 23°S by Kirchhoff et al. (1981) and later by Takahashi et al. (1992) at the same location. Thomas et al. (1984) and Thomas (1990) show
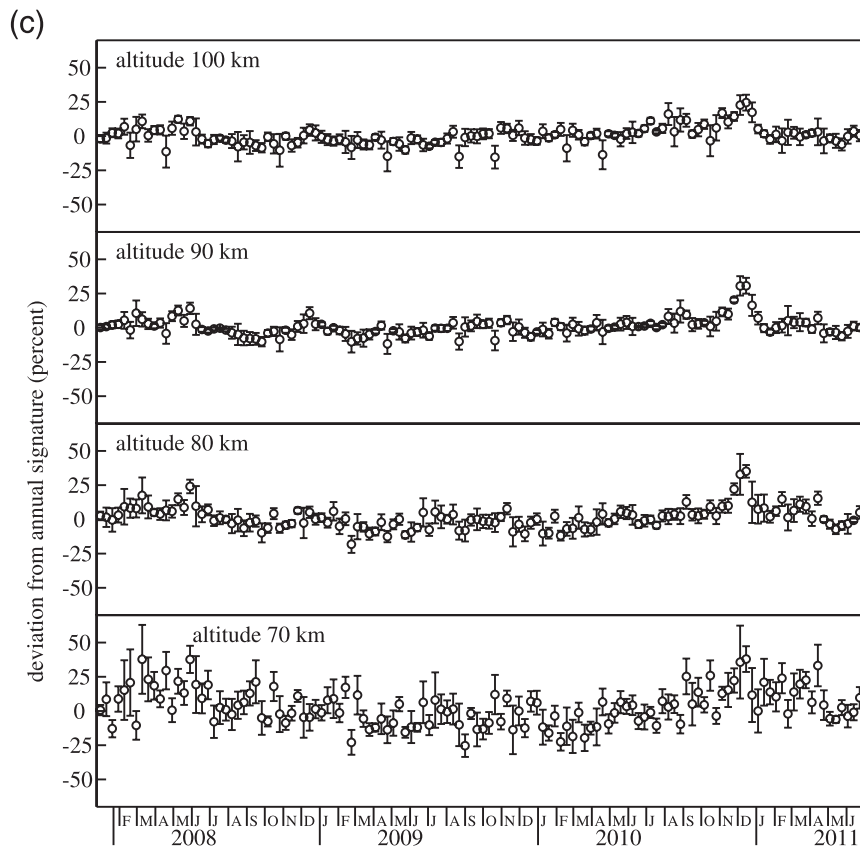
(c)

Fig. 6. (*Continued*)

the seasonal variation of ozone from the Solar Mesosphere Explorer (SME) above 80 km altitude to be very repeatable from year to year. The SME data, which cover a wide range of latitude, show a higher concentration in the spring equinox than in the fall for 45°N latitude, although the concentration becomes more equal at each equinox at 38°N. The ozone data from the SABER instrument reported by Smith et al. (2008) shows high ozone mixing ratios above 18 ppmv in April and late October each year. The comparison of the SABER and MOSAIC data shown in Figs. 5a and 5b shows fairly good agreement within the expected errors in the MOSAIC data discussed in the previous section. In addition, the deviation in the yearly trend in late 2010 is clearly present in both sets of data. However, the minima in January each year are less pronounced in the MOSAIC data.

Observations of the semiannual variations of ozone from the Global Ozone Monitoring by Occultation of Stars (GOMOS) instrument on the *Envisat* satellite for 2002–08 are shown by Kyrola et al. (2010). The results shown in Fig. 9 of Kyrola et al. (2010), for a latitude range of 40°–50°N, show a peak number density of about

6×10^8 cm^{-3} at the peaks following the equinoxes, corresponding to 11 ppmv at 90 km assumed for a fit based on an assumed temperature of 190 K and pressure of 0.001 hPa at 92 km. These results have an annual signature whose maxima and minima match those from MOSAIC to within about 5% after a scale adjustment of about 25%. The minima in January are in much better agreement with those of the MOSAIC data than with the SABER data.

We also note Kyrola et al. (2010) find that the peak ozone concentrations are a little higher following the autumnal equinox, as is seen in the SABER and MOSAIC data. We explored the latitude and longitude dependence of the SABER data and found that averaging over 40° to 50°N, as in the GOMOS data from Kyrola et al. (2010), raises the minima in January by about 10% which is less than the 20% needed to make the annual signature from SABER agree with that of the MOSAIC and GOMOS data.

We found no significant dependence on longitude in the SABER data, and the significantly higher mixing ratio seen in the MOSAIC data in late 2010, discussed further in section 8, is seen in the SABER data for each quadrant of longitude.

7. Seasonal variation model

The Research for Ozone in the Stratosphere and its Evolution (ROSE) model of Smith and Marsh (2005), which is based on primitive equations with interactive chemistry, predicts the ozone concentration at night from the balance between the creation via collisions of atomic oxygen with molecular oxygen and a third catalytic molecule, such as nitrogen, and destruction by reactions with atomic hydrogen. During the day mesospheric ozone above 80 km is almost completely destroyed by solar ultraviolet radiation which breaks ozone into atomic and molecular oxygen. The chemistry of the ROSE model predicts that seasonal variation of ozone will be largely controlled by the seasonal variation in atomic hydrogen. Takahashi et al. (1992) obtain semiannual variations of atomic hydrogen and ozone, from observations taken at 22.7°S, 45.0°W, with opposite phase from the upper mesospheric airglow emission intensities of atomic oxygen, sodium (NaD lines) and OH. Lossow et al. (2008) show a semiannual variation in mesospheric water vapor, suggesting that the variation of atomic hydrogen is due to the seasonal variation of water vapor, which is broken into atomic hydrogen and the hydroxyl radical by solar ultraviolet radiation during the day. The ROSE model, which is supported by the observations of Takahashi et al. (1992) and Lossow et al. (2008), agrees with the general trends of the seasonal variations of mesospheric ozone seen in the data from MOSAIC, SABER, and GOMOS.

8. Higher ozone concentration in late 2010

The departure from the average yearly signature in late 2010 MOSAIC is the most significant deviation from the yearly trend observed on this averaging scale. The increased ozone concentration over the average signature persists for each 10-day average from mid-November 2010 until the end of December 2010. On average, the increase is about 25% over the same period in previous years. To explore the extent of this anomaly the residual variation after removal of the annual signature in the SABER data was studied for a range of latitudes, longitudes, and altitude. Figure 6a shows the fractional deviation from the annual signature for five 30° wide bands of latitude centered at 60°S, 30°S, 0°, 30°, and 60°N for an altitude of 95 km. From this plot it is clear that the anomaly extends from high latitudes in the north down to about 30° south. Below 30° south the high ozone in late 2010 appears to split into a double feature with anomalously high ozone in August 2010 while data in late 2010 is noisy owing to the reduced duration of nighttime data in the austral summer. Figure 6b shows that there is no significant change in the high ozone in

late 2010 with longitude as the anomaly appears about equally in four 90° wide bands centered at 0, 90, 180, and 270 degrees for a band of latitude from 30°S to 60°N. Figure 6c shows the deviation of the annual signature obtained from global average SABER data for altitudes centered at 70, 80, 90, and 100 km. Figures 6a,b,c show that the higher than normal ozone in late 2010 is of global extent and covers a range of altitudes from 80 to 100 km.

One possible mechanism for the significant duration above the otherwise highly repeatable yearly signature is a global change in the atmospheric circulation. Sassi et al. (2004) show that the El Niño–Southern Oscillation (ENSO) phenomenon influences the general circulation in the middle atmosphere and has effects extending into the mesosphere. Both the Southern Oscillation index (SOI) and the Niño ENSO indices point to a strong La Niña event in late 2010, with the Oceanic Niño index (ONI) running below −1.0°C for the months of September 2010 through February 2011.

Effects of strong sudden stratospheric warming (SSW) events have also been reported to influence the ozone concentration in the mesosphere by Sridharan et al. (2012), but there is no evidence for a major SSW event in November or December 2010 so it is unlikely that the increased ozone seen in late 2010 is due to an SSW event. Space weather events, like solar proton events, are also known to affect the ozone concentration in the mesosphere. However, these events are very unlikely to have any effect at midlatitudes and these events are likely to deposit increased numbers of protons in the mesosphere, which would reduce the ozone concentration rather than produce an increase as observed (Jackman and McPeters 2004).

It may be significant that the increased concentration comes at a time when the ozone concentration is declining most rapidly, possibly as a result of water vapor carried by the meridional flow from the southern pole. If this flow was delayed compared with other years, the ozone concentration would be higher at this time. An indication of a delay in the meridional flow comes from SABER data of the temperature at 90 km above the southern polar region. These data show that temperatures in the 160-K range are only reached at the end of November 2010 whereas in 2008 and 2009 160 K is reached at least 10 days earlier. To examine this possibility further we obtained temperature data from the Earth Observing System (EOS) Microwave Limb Sounder (MLS) for the mesosphere above the Antarctic. This MLS data provides full coverage the southern polar region compared with the limited data from SABER. Figure 7 shows the departure of temperature from the annual signature obtained from the residuals to a Fourier series with 1-yr period in the same manner as used to illustrate
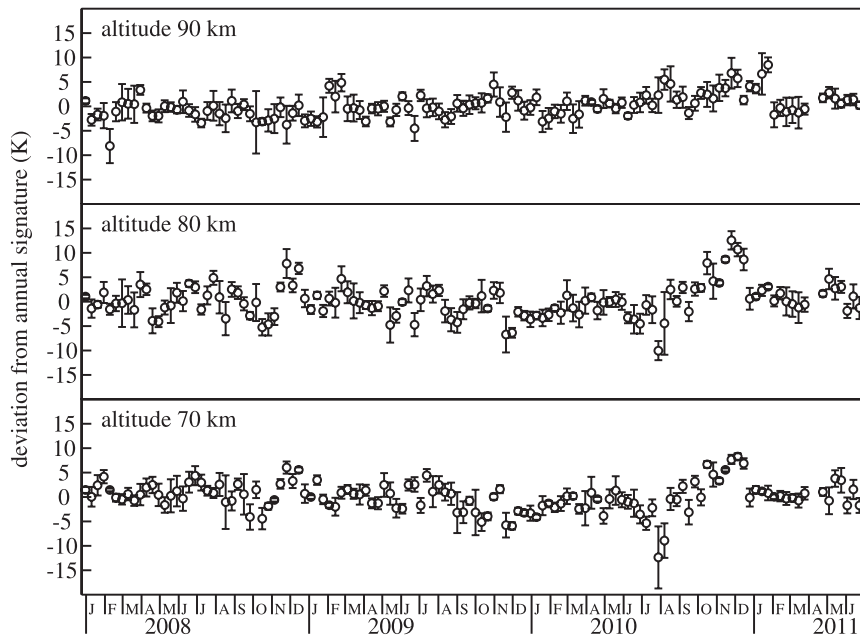
FIG. 7. Deviation of the temperature of the mesosphere from the annual signature for latitudes south of 70°S from the MLS data for altitudes of 70, 80, and 90 km.

the higher than normal level of mesospheric ozone in observed in late 2010. This clearly shows that the normally low temperatures above the Antarctic in the austral summer arrived later in 2010 than in other years. Since these low temperatures are produced by the adiabatic expansion of the rising air from the summer pole on its way to the winter pole via the mesosphere the late arrival of low temperatures indicates a delay in the meridional flow.

The increased ozone concentration at 38°N in late 2010 could also be due to a lower than normal temperature in the region. The ratio of temperature dependence T of ozone creation (via the three-body collisions) to the destruction (via reaction with atomic hydrogen) from Smith and Marsh (2005) is

$$T^{-2.4} \exp(470/T).$$

This implies that a drop in the average late November temperature from 180 to 170 K at 90 km would result in a 30% increase in nighttime ozone. However, we could find no evidence for significant differences in temperature, at the level of 2 K, from SABER data in the 90–95-km range at 38°N for November/December 2010 compared with 2008 and 2009. We also examined the variation of the height of the maximum in ozone mixing ratio above 80 km in the SABER data and found no significant change associated with the increase in late 2010.

9. Conclusions

The seasonal variation of ozone above 80 km is very repeatable from year to year with asymmetric peaks in April and late October each year for a latitude of 38°N. The times of these peaks coincide with minima in the concentration of water vapor in the high mesosphere, and are consistent with models in which the concentration is largely determined by atomic hydrogen, formed from the breakdown of water vapor during the day by solar ultraviolet radiation. The ozone concentration in December 2010 is significantly higher than the largely repeatable yearly signature and an examination of the ozone concentration in the mesosphere derived from the SABER shows that this anomaly is of global scale. If the ozone concentration is controlled by water vapor carried by the interhemispheric meridional flow, then a significant delay in establishing the meridional flow from the South Pole in late 2010, as suggested by the temperature data, would result in the observed increase of ozone over the yearly average. The cause of the change in flow is most likely the result of changes in the circulation of the lower atmosphere, although further study of the coupling is needed.

in the acquisition of the data. We also thank Jason Soohoo and Richard Crowley for their help in setting up the automated retrieval of the data each day via internet connections. In addition, we also thank M. Lekberg, J. Cadigan, and M. Needles for their work in starting the MOSAIC project. We are deeply indebted to the reviewers of our paper who motivated us to obtain the large SABER and MLS datasets for comparison. We acknowledge and thank the SABER and EOS MLS teams for making their data available via the Internet.

APPENDIX

Calculation of Model Spectra

a. Radiative transfer

If we assume the ozone is in local thermodynamic equilibrium with the kinetic temperature T_{kinetic}, the brightness temperature of a ray entering the ozone T_{in} is attenuated by the optical depth τ, while the ray acquires the fraction $1 - e^{-\tau}$ of the kinetic temperature so that the outgoing ray has the brightness temperature T_{out} given by

$$T_{\text{out}} = T_{\text{in}} e^{-\tau} + T_{\text{kinetic}}(1 - e^{-\tau}). \tag{A1}$$

Since the optical depth of the 11-GHz line is very small and T_{in} is close to the 3-K cosmic microwave background temperature, the brightness temperature due to the line optical depth is approximately

$$T_{\text{out}} = (T_{\text{kinetic}} - T_{\text{cmb}})\tau \tag{A2}$$

using the Taylor series expansion.

b. Path through the atmosphere

The pathlength, $\text{len}(h)$ in kilometers, through a layer of 1-km thickness at a height h is given by the difference of the pathlength to the upper and lower boundaries of the layer from the derivative

$$\frac{d\text{len}(h)}{dh} = (R + h)[R^2 \sin^2(\phi) + 2Rh + h^2]^{-1/2}, \tag{A3}$$

where ϕ is the antenna elevation, and R is the radius of the earth as illustrated in Fig. 1b. For low altitudes the pathlength is approximately $\sin^{-1}(\phi)$ or 7.2 km. At an altitude of 95 km the pathlength is reduced to 4.5 km owing to the curvature of the earth.

c. Doppler-line shape

The line shape from the free motion of the ozone molecules is given by

$$\text{shape}(f) = e^{-0.693 f^2 / w^2}, \tag{A4}$$

where f is the frequency, and w is the half-power half-width given by

$$w = f\text{line}[2 \ln(2)kT/m]^{1/2}/c, \tag{A5}$$

where $f$line is the ozone line frequency, k is Boltzmann's constant, T is the kinetic temperature, m is the molecular weight of ozone, and c is the velocity of light. The half-power half-width is 7.9 kHz at 190 K.

d. Line shape

The line shape is the convolution of the Doppler shape with the Lorentz shape

$$\text{shape}(f) = [(p_w/\pi)/(f^2 + p_w^2)] \oplus e^{-0.693 f^2 / w^2}, \tag{A6}$$

where p_w is the pressure width.

e. Integrated line intensity

The integrated line intensity at 300 K is $10^{-6.9997}$ nm^2 MHz from the JPL tables.

f. Line intensity corrected for temperature

The line intensity from the JPL tables is corrected for temperature using the factors of Eq. (A11) of Rothman et al. (1998). At 11 GHz the expression becomes

$$I(T) = I(300)\left[\frac{Q(300)}{Q(T)}\right]\left(\frac{e^{-c2E/T}}{e^{-c2E/300}}\right)\left(\frac{300}{T}\right), \tag{A7}$$

where I is the integrated line intensity, $Q(T)$ is the total internal partition function, $c2$ is constant 1.4388 cm K, and E is the energy of the lower state of 8.0217 cm^{-1}.

g. Conversion from volume mixing ratio ppmv to number density

$$n = (6.022 \times 10^{23}) \times (1.293 \times 10^{-3})$$
$$\times (273/T) \times P \times (V \times 10^{-6})/28.97, \tag{A8}$$

where n is the density (molecules cm^{-3}), P is the pressure in atmospheres, V is the volume mixing ratio in ppmv, 6.022×10^{23} is Avogadro's number (molecules mol^{-1}), 1.293×10^{-3} is the weight of 1 atmosphere of air at 273 K (g cm^{-3}), and 28.97 (g mol^{-1}) is the total molecular mass of air. Here, $V = 1$ for the model spectrum below 80 km and

$$V = e^{-0.693(h-95)^2/5^2} \tag{A9}$$

for the model spectrum above 80 km.

h. Adding up the layers

The layers of the atmosphere are added with an integral which is approximated with the sum

$$T(f) = \sum_{h=10}^{h=100} [T_{\text{kinetic}}(h) - T_{\text{cmb}}]\tau(h,f)\text{len}(h) \times 10^5,$$

(A10)

where $\tau(h,f)$ is obtained from the product of the line intensity $I(T)$, the line shape, and the ozone density n obtained from Gaussian weighting function assumed for the ozone mixing ratio

$$\tau(h,f) = 10^{-14} \times I(T) \times n \times \text{shape}(f), \quad (A11)$$

where the numerical factors of 10^{-14} and 10^5 convert nm^2 to cm^2 and km to cm, respectively.

i. Ozone spectrum

The ozone spectrum in kelvins $S(f)$ is then derived from the product of brightness temperature and the beam efficiency B_{eff}:

$$S(f) = B_{\text{eff}}T(f). \quad (A12)$$

REFERENCES

Houghton, J., 2007: The general circulation. *The Physics of Atmospheres,* Cambridge University Press, 145–172.

Jackman, C. H., and R. D. McPeters, 2004: The effects of solar proton events on ozone and other constituents. *Solar Variability and Its Effects on Climate, Geophys. Monogr.,* Vol. 141, Amer. Geophys. Union, 305–319.

Kirchhoff, V. W. J. H., B. R. Clemesha, and D. M. Simonich, 1981: Seasonal variation of ozone in the mesosphere. *J. Geophys. Res.,* **86** (A3), 1463–1466.

Kyrola, E., and Coauthors, 2010: GOMOS O$_3$, NO$_2$, and NO$_3$ observations in 2002–2008. *Atmos. Chem. Phys.,* **10,** 7723–7738.

Lossow, S., J. Urban, J. Gumbel, P. Eriksson, and D. Murtagh, 2008: Observations of the mesospheric semi-annual oscillation (MSAO) in water vapor by Odin/SMR. *Atmos. Chem. Phys.,* **8,** 6527–6540.

Pickett, H. M., R. L. Poynter, E. A. Cohen, M. L. Delisky, J. C. Pearson, and H. S. P. Muller, 1998: Sub-millimeter, millimeter, and microwave spectral line catalog. *J. Quant. Spectrosc. Radiat. Transfer,* **60,** 883–890.

Rogers, A. E. E., M. Lekberg, and P. Pratap, 2009: Seasonal and diurnal variations of ozone near the mesopause from observations of the 11.072-GHz line. *J. Atmos. Oceanic Technol.,* **26,** 2192–2199.

Rothman, L. S., and Coauthors, 1998: The HITRAN molecular spectroscopic database and HAWKS (HITRAN Atmospheric workstation): 1996 edition. *J. Quant. Spectrosc. Radiat. Transfer,* **60,** 665–170.

——, and Coauthors, 2005: The HITRAN 2004 molecular spectroscopic database. *J. Quant. Spectrosc. Radiat. Transfer,* **96,** 139–204.

Sassi, F., D. Kinnison, B. A. Boville, R. R. Garcia, and R. Roble, 2004: Effect of El Niño–Southern Oscillation on the dynamical, thermal, and chemical structure of the middle atmosphere. *J. Geophys. Res.,* **109,** D17108, doi:10.1029/2003JD004434.

Shambayati, S., 2008: Atmosphere attenuation and noise temperature at microwave frequencies. *Low-Noise Systems in the Deep Space Network,* MacGregor S. Reid, Ed., John Wiley and Sons, 255–280.

Smith, A. K., and D. R. Marsh, 2005: Processes that account for the ozone maximum at the mesopause. *J. Geophys. Res.,* **110,** D23305, doi:10.1029/2005JD006298.

——, ——, J. M. Russell III, M. G. Mlynczak, F. J. Martin-Torres, and E. Kyrola, 2008: Satellite observations of high nighttime ozone at the equatorial mesopause. *J. Geophys. Res.,* **113,** D17312, doi:10.1029/2008JD010066.

Sridharan, S., S. Sathishkumas, and S. Gurubaran, 2012: Variabilities of mesospheric tides during sudden stratospheric warming events of 2006 and 2009 and their relationship to ozone and water vapour. *J. Sol. Terr. Phys.,* **78–79,** 108–115.

Takahashi, H., B. R. Clemesha, Y. Sahai, P. P. Batista, and D. M. Simonich, 1992: Seasonal variations of mesospheric hydrogen and ozone concentrations derived from ground-based airglow and lidar observations. *J. Geophys. Res.,* **97** (D5), 5987–5993.

Thomas, R. J., 1990: Seasonal ozone variations in the upper mesosphere. *J. Geophys. Res.,* **95** (D6), 7395–7401.

——, C. A. Barth, and S. Solomon, 1984: Seasonal variations of ozone in the upper mesosphere and gravity waves. *Geophys. Res. Lett.,* **11,** 673–676.